Applied Thermal Engineering 162 (2019) 114227

Contents lists available at ScienceDirect

Applied Thermal Engineering

journal homepage: www.elsevier.com/locate/apthermeng

# The effect of liquid charge ratio on organic Rankine cycle operation

Shuang Cao[b], Zheng Miao[a,*], Jinliang Xu[a]

[a] The Beijing Key Laboratory of Multiphase Flow and Heat Transfer, North China Electric Power University, 102206 Beijing, China
[b] School of Energy and Power Engineering, Zhengzhou University of Light Industry, Zhengzhou 450002, Henan, China

## HIGHLIGHTS

- The effect of liquid charge ratio on ORC operation was experimentally studied.
- An optimal liquid charge ratio 42.5% was determined to achieve the best system performance.
- Pump cavitation may occur to deteriorate the performance below the optimal charge ratio.
- Condenser pressure rises to deteriorate the system performance above the optimal charge ratio.
- We present important criterion of liquid charge ratio to optimize the system operation.

## ARTICLE INFO

*Keywords:*
Organic Rankine cycle
Liquid charge ratio
Pump
Condenser
System efficiency

## ABSTRACT

Liquid charge ratio is defined as the total liquid volume charged in an organic Rankine cycle (ORC) system divided by the total internal volume of the system, which influences the two-phase (vapor-liquid) phase distribution to dominate the component operation. In this paper, the effect of liquid charge ratio on ORC performance is explored for a ~10 kWe ORC system. It is shown that ORC can operate with liquid charge ratios in the range of 35–50%. At an optimal liquid charge ratio of 42.5%, the system attains the maximum thermal efficiency, power efficiency and net efficiency of 7.74%, 7.02% and 5.62%, respectively. When the system operates below the optimal liquid charge ratio of 42.5%, the liquid flushing may occur to induce pump cavitation and unstable flow due to insufficient liquid suction during pumping process. Alternatively, when the system operates above the optimal liquid charge ratio of 42.5%, more liquid is occupied in the condenser, decreasing the effective heat transfer area to elevate the condensation pressure, thus the system efficiency is worsened. This paper presents the important criterion for optimal liquid charge ratio for ORC operation.

## 1. Introduction

The global energy shortage and environmental issues inspire us to develop new energy utilization technologies [1,2]. The utilization of low-grade heat has attracted more and more attentions. Organic Rankine cycle (ORC) is regarded as one of the key technologies to convert low grade heat source such as waste heat [3,4], solar energy [5–7], biomass energy [8–10] and geothermal energy [11–13] into work. ORC has the similar thermodynamic configuration of the steam Rankine cycle, but use the organic working fluid with low boiling temperature instead of water to generate higher pressure at low temperature heat sources [14].

The ORCs have been intensively studied theoretically and experimentally during the past two decades. Theoretical works mainly focus on the thermodynamic analysis [15–17], selection of working fluids [18–21], configuration modification [22,23], and control model development [24–26]. Theoretical results have provided lots of useful reference for the ORC design. However, the ideal assumptions used in the theoretical analysis make the predicted performance deviating from the actual operating performance. Consequently, it is of great importance to develop experimental setup of ORCs for the investigation of its actual operation characteristics and control strategy [27,28].

The experimental testing provides basic data of the ORC system operation and performance. The objective is to study the off-design performance of the system and achieve the optimum design parameters for long time operation under specific heat source. Most reported experimental setup are small-scale ORCs (1–10 kW power output) [29–35]. Jang and Lee [29] investigated the effects of external parameters on the compact ORC performance. They found the electrical output can be well predicted by the pressure difference rather than the

* Corresponding author.
*E-mail address:* miaozheng@ncepu.edu.cn (Z. Miao).

https://doi.org/10.1016/j.applthermaleng.2019.114227
Received 16 May 2019; Received in revised form 14 July 2019; Accepted 7 August 2019
Available online 08 August 2019
1359-4311/ 

**Nomenclature**

| | |
|---|---|
| $E$ | exergy [kW] |
| $h$ | specific enthalpy or [kJ/kg] |
| $I$ | exergy destruction [kW] |
| $m$ | mass flow rate [kg/h] |
| $n$ | rotating speed [rpm] |
| $P$ | pressure [kPa] |
| $Q$ | heat transfer rate [kW] |
| $R$ | expander inlet and outlet pressure ratio |
| $s$ | entropy [kJ/(kg·K)] |
| $T$ | temperature [°C] |
| $V$ | volume flow [$m^3$/h] |
| $VCR$ | working fluid charge ratio [%] |
| $W$ | power [kW] |

*Greek symbols*

| | |
|---|---|
| $\eta$ | efficiency[%] |
| $\Delta T$ | degree of superheating or subcooling [°C] |

*Subscripts*

| | |
|---|---|
| con | condenser |
| eva | evaporator |
| exp | expander |
| ele | electric |
| in | inlet |
| net | net power |
| out | outlet |
| oil | conductive oil |
| ORC | organic Rankine cycle |
| p | pump |
| r | working fluid (R245fa fluid in this study) |
| s | isentropic |
| sub | subcooling |
| sup | superheating |
| th | thermal |
| tank | liquid tank |
| w | cooling water |

expansion ratio of the expander. The generator efficiency is only linearly proportional to the electrical power. The maximum electrical output and thermal efficiency were 0.15 kW and 1.61%, respectively. Feng et al. [30] examined the effect of lubricant oil ratio under three different superheating degrees. Results show that the lubricant oil enhances the pump behavior but deteriorates the expander shaft power and electrical power. Bianchi et al. [31] presented an experimental study on a micro-ORC system driven by a piston expander. The expander total efficiency showed a barely constant trend around 40% and the maximum net efficiency was 2.2% at the heat source temperature of 85 °C. Dumont et al. [32] proposed an experimental test in two small-scale ORC test rigs using four different volumetric expanders (namely scroll, screw, roots and piston). The calibration of semi-empirical models based on experimental results were developed to predict the isentropic efficiencies of expanders in optimal conditions. In our previous research, we used two independent parameters: the working fluid mass flow rate and the external load to control the operation of ORCS, and it is found that the measured pump consumed powers were 2–4 times higher than the calculated ones [33]. Subsequently, the cavitation mechanisms of the expander and working fluid pump were investigated. A vapor superheating of 13 °C at expander inlet and a liquid subcooling of 20 °C at pump inlet are necessary to avoid cavitation [34]. The match between the ORC power capacity and the external load was analyzed in our recent study [35]. In addition, a control strategy was proposed in the current work to achieve better system performance at varied external parameters.

The working fluid charge ratio ($VCR$), which is defined as the ratio of the liquid working fluid charge volume ($V_r$) to the internal volume of ORC unit ($V_{ORC}$), was found have a significant impact on the thermodynamic and economic performance of the cycle, especially for the system working under the violent fluctuating heat source or ambient temperature. The first study of ORC working fluid charge ratio is reported by Li et al. [36]. The results showed that different working fluid had different optimal charge ratio. R245fa had the optimal charge ratio of 38%, whereas the R245fa/R601a mixture had 41%. Kim et al. [37] noted that the charge amount cannot be limitlessly used to enhance the system power output. With the increasing working fluid charge ratio, the power of expander and pump both increases. The faster rise of pump power than expander power was tested. Thus, a maximum net power of output is eventually reached at the optimal charge ratio of 32.6%. Liu et al. [38] found that the pump performance can be significant improved by overcharging working fluid, whereas the working fluid charge has slightly effect on the output power of the expander. However, the relationship between working fluid charge, pump cavitation and the liquid level in working fluid tank has not been sufficiently studied. On the aspect of theory, Ziviani et al. [39] developed a charge-sensitive cycle model, which provides insight into the behavior of a specific installation at different refrigerant-charge levels and the impact on the subcooling level. Liu et al. [40] established a working fluid charge oriented model and calculated the theoretical value of working fluid charge level for the system under rated condition. They found that the system with lower working fluid charge amount required higher degree of superheating at the expander inlet and the highest thermal efficiency reached 6.37% with the optimal working fluid charge amount of 34.6 kg. Dickes et al. [41] proposed a charge-sensitive ORC model for off-design performance simulations. A dedicated two-stage solver was developed to overcome the convergence issues which is caused by the presence of a liquid receiver. The predicted values were well matched with the experimental measurements.

The literature review above reveals that the studies on the effect of the working fluid charge ratio are still on the infancy stage. Although some previous studies investigated the effect of the working fluid charge ratio, the focus was limited to the performance of ORC systems [36,37] and the change of dynamic liquid holdup of the system [39–41]. Few literature explain the main mechanism of the effect of working fluid charge ratio, as the pump cavitation mechanism and liquid flooding in the condenser were not quantitative and qualitative analyzed due to the lack of experimental data. More effort should be dedicated to this topic to shed light on the mechanism. The objective of the present work is to experimentally study the working fluid charge ratio effects on the operation and performance of the ORC system. A 7.5 kW scale ORC prototype using single screw expander is developed and tested. The expander rotating speed and heat source temperature are kept at 3000 rpm and 115 °C, respectively. External loads cover the range of 1.5–6.0 kW. Operation characteristics are investigated at the working fluid charge ratio range of 35–50%. The tank liquid height is measured to explore the system working fluid charge level which may cause the pump cavitation or liquid flooding in the condenser.

## 2. Experimental system

### 2.1. ORC prototype design

Fig. 1 shows the schematic diagram of the designed ORC prototype. This system consists of three coupled subunits which represented by

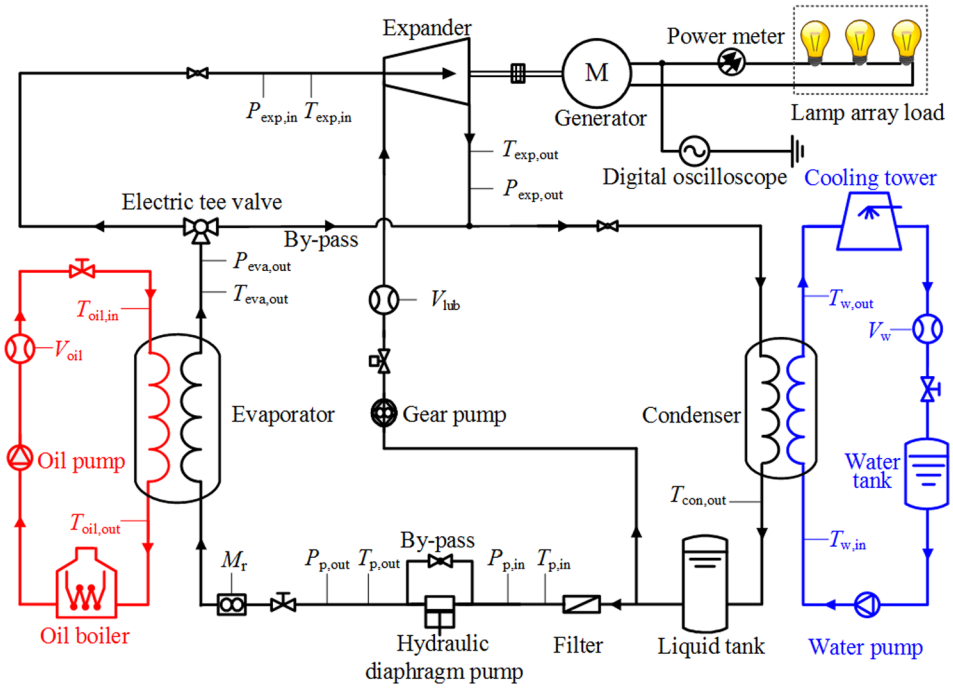


**Fig. 1.** Schematic diagram of ORC system.

different colors: ORC loop (black line), heat conductive oil loop ([1]red line) and cooling water loop (blue line).

#### 2.1.1. The ORC loop

The photo of the ORC loop is shown in Fig. 2a. A working fluid pump, a liquid tank, an electric Tee valve, an evaporator, a generator, an expander, and a condenser are involved in this loop. R245fa was used as working fluid due to its better thermal efficiency and environmental performance [42]. The height of liquid R245fa in the tank is measured by a magnetic floater liquid level meter. The mass flow rate ($m_r$) is controlled by a frequency converter and measured by a Coriolis mass flow meter. The liquid working fluid is pumping into an evaporator to generate high pressure vapor which drive the expander to produce work. Then, the low pressure vapor at the expander outlet is condensed to liquid in a condenser.

Fig. 2b shows the photo of the single screw expander. The single screw expander has the advantages of the axial force balance of main rotor. And it can operate in a wide range of power capacities [35,43]. It is considered as one of the promising candidates for the expander of ORCs. In the present work, the expander was modified from a commercial compressor. The designed shaft power of the expander is about 7.5 kW. An electric tee valve is installed to either operate or by-pass the expander by switching the R245fa vapor to flow in different pipes. A three-phase synchronous generator is connected coaxially with the expander by an elastic coupling to generate electricity. The generator has the rated rotating speed of 3000 rpm and the maximum output power of 11 kW. The electricity generated by the generator is measured by a power meter and consumed by the halogen lamps array (see Fig. 2c).

Plate heat exchanger is widely used in small scale ORC system due to its high heat transfer coefficient, low investment cost and convenient setting [44]. In this prototype, two plate heat exchangers with the heat transfer area of 35.9 $m^2$ and 12.3 $m^2$ are used as the evaporator and condenser, respectively. Both rated heat loads of the evaporator and condenser are 120 kW. Fig. 3 shows the internal structure of the plate heat exchangers. The plates used for the corrugated gap having a mean corrugation depth of 2.8 mm, a width of 0.4 mm and a corrugation angle of 60°.

#### 2.1.2. The heat conductive oil loop

Fig. 2d shows the photo of a 100 kW oil boiler, which can automatically adjust the heating power to maintain the required oil temperature entering ORC with an uncertainty of 1 °C. The heat conductive oil loop is thermally coupled with the ORC evaporator to heat the R245fa fluid. The oil is circulated by the pump and the flow rate is controlled by the adjustment valve and measured by a target flow meter.

#### 2.1.3. The cooling water loop

The cooling water loop is shown in Fig. 2e. A 150 kW cooling tower is the key component of the loop. The flow rate of cooling water is measured by a turbine flow meter. The cooling water temperatures at the condenser inlet and outlet are also measured to monitor the cooling water loop operation.

### 2.2. Thermodynamic equations

During the operation, the heat absorbed in the evaporator is:

$$Q_{eva} = m_r (h_{eva,out} - h_{p,out}) \quad (1)$$

where $h_{eva,out}$ and $h_{p,out}$ are R245fa enthalpies based on the measured temperatures and pressures at the outlet of evaporator and pump, respectively.

The heat release in the condenser is:

$$Q_{con} = m_r (h_{exp,out} - h_{con,out}) \quad (2)$$

where $h_{exp,out}$ and $h_{con,out}$ are R245fa enthalpies at the outlet of expander and condenser, respectively.

The calculated shaft power of the expander is:

$$W_{th} = m_r (h_{exp,in} - h_{exp,out}) \quad (3)$$

where $h_{exp,in}$ and $h_{exp,out}$ are the R245fa enthalpies based on measured temperatures and pressures at expander inlet and outlet.

The pump isentropic efficiency is defined as:

[1] For interpretation of color in Fig. 1, the reader is referred to the web version of this article.

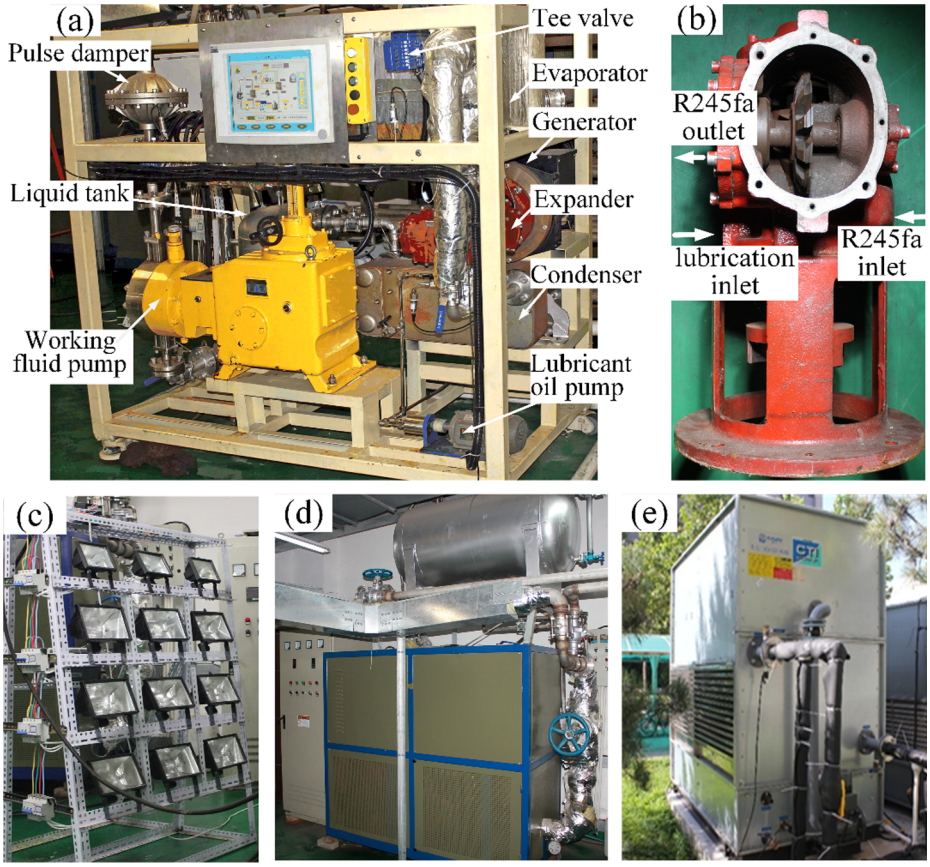


**Fig. 2.** Photos of experimental setup: (a) ORC unit, (b) single screw expander, (c) load system, (d) conductive oil loop and (e) cooling water loop.

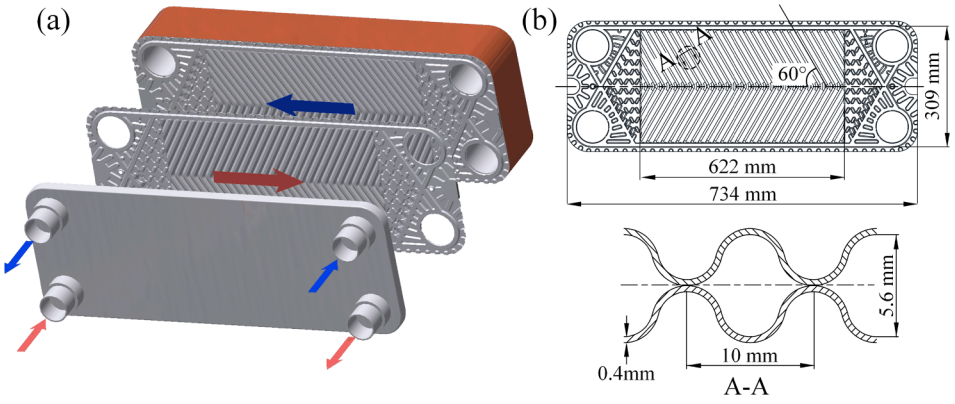


**Fig. 3.** Structure of plate heat exchanger.

**Table 1**
Major parameters, instruments and uncertainties.

| Parameters | Instruments | Uncertainties |
|---|---|---|
| Temperature (°C) | KMQXL-040G-6 | ± 0.5 °C |
| Pressure (kPa) | CYT-103 | 0.2% |
| R245fa mass flow rate (kg/h) | DMF-1 | 0.2% |
| Conductive oil flow rate ($m^3$/h) | YD-LBL-65 | 0.5% |
| Cooling water flow rate ($m^3$/h) | YD-LWGY-50 | 0.5% |
| Lubricant flow rate ($m^3$/h) | YD-LWGY-10 | 0.5% |
| Electric power (kW) | AKW91110 | 0.5% |
| Electric frequency (Hz) | AKW91110 | 0.2% |
| Pumping power (kW) | ACS510 | 2% |

**Table 2**
Running cases of the experiment.

| Parameter | Value |
|---|---|
| $T_{oil,in}$ (°C) | 115 |
| $T_{w,in}$ (°C) | 10 |
| $V_{oil}$ ($m^3$/h) | 13.07 ± 0.46 |
| $V_w$ ($m^3$/h) | 12.27 ± 0.33 |
| *VCR* (%) | 35.0, 37.5, 40.0, 42.5, 45.0, 47.5, 50.0 |
| $n_{exp}$ (rpm) | 3000 |
| *Load* (kW) | 1.5, 3.0, 4.5, 6.0 |

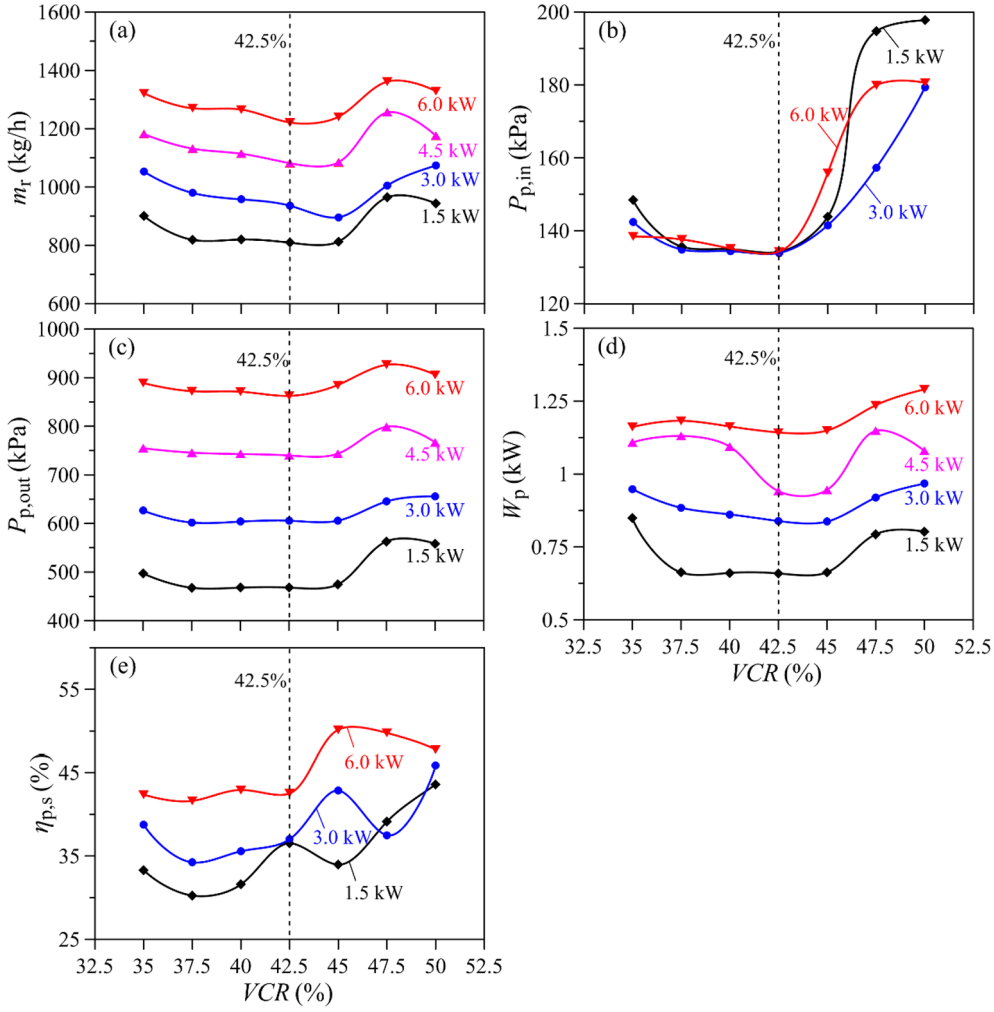


**Fig. 4.** Parameters and performance of working fluid pump versus *VCR* at $T_{oil,in}$ = 115.1 °C, $n_{exp}$ = 3000 rpm, $V_{oil}$ = 13.19 $m^3$/h, $V_w$ = 12.44 $m^3$/h.

$$\eta_{p,s} = \frac{h_{p,out,s} - h_{p,in}}{h_{p,out} - h_{p,in}} \times 100\% \quad (4)$$

where $h_{p,in}$ and $h_{p,out}$ are the R245fa enthalpies based on measured temperatures and pressures at pump inlet and outlet, $h_{p,out,s}$ is the pump outlet enthalpy based on isentropic compression.

The pressure ratio and isentropic efficiency of the expander are:

$$R = P_{exp,in}/P_{exp,out} \quad (5)$$

$$\eta_{exp,s} = \frac{h_{exp,in} - h_{exp,out}}{h_{exp,in} - h_{exp,out,s}} \times 100\% \quad (6)$$

where $P_{exp,in}$ and $P_{exp,out}$ are the expander inlet and outlet pressures, $h_{exp,out,s}$ is the expander outlet enthalpy based on isentropic expansion.

The thermal efficiency, electric power efficiency and net efficiency of the ORC system are defined as:

$$\eta_{th} = \frac{W_{th}}{Q_{eva}} \times 100\% \quad (7)$$

$$\eta_{ele} = \frac{W_{ele}}{Q_{eva}} \times 100\% \quad (8)$$

$$\eta_{net} = \frac{W_{ele} - W_p}{Q_{eva}} \times 100\% \quad (9)$$

where $W_{ele}$ is electric power directly measured by an electric power meter. $W_p$ is pumping power measured by a frequency converter.

To generalize the irreversible loss of each component, the exergy analysis of the components is performed. The exergy at any state point is given as:

$$E = m_r[(h - h_0) - T_0(s - s_0)] \quad (10)$$

where $h$ and $s$ are the enthalpy and entropy at specific state. The subscript 0 refers to the reference state and is set as $T_0$ = 293.15 K and $P_0$ = 101.3 kPa. Thus, the exergy destruction for a specific component is computed as:

$$I = E_{in} - E_{out} \quad (11)$$

High quality sensors and instruments are used in the prototype to measure temperatures, pressures, cycling flow rates and electric power (see Fig. 1). Table 1 summarized the uncertainties of the major instruments. The uncertainties of parameters in equations mentioned above are determined by directly measured parameters and evaluated on the basis of the error transmission theory [45]. In this study, the thermal efficiency, electric power efficiency and net efficiency have accuracies of 5.27%, 3.96% and 4.12%, respectively.

### 2.3. The operating procedure

The ORC operation is controlled by adjusting the electric load and R245fa mass flow rate under different charge ratio. Table 2 shows the operating parameters. The inlet temperatures of conductive oil and cooling water are kept as 115 °C and 10 °C, respectively. The flow rate of conductive oil and cooling water are 13.07 ± 0.46 $m^3$/h and 12.27 ± 0.33 $m^3$/h, respectively. The expander rotating speed is kept

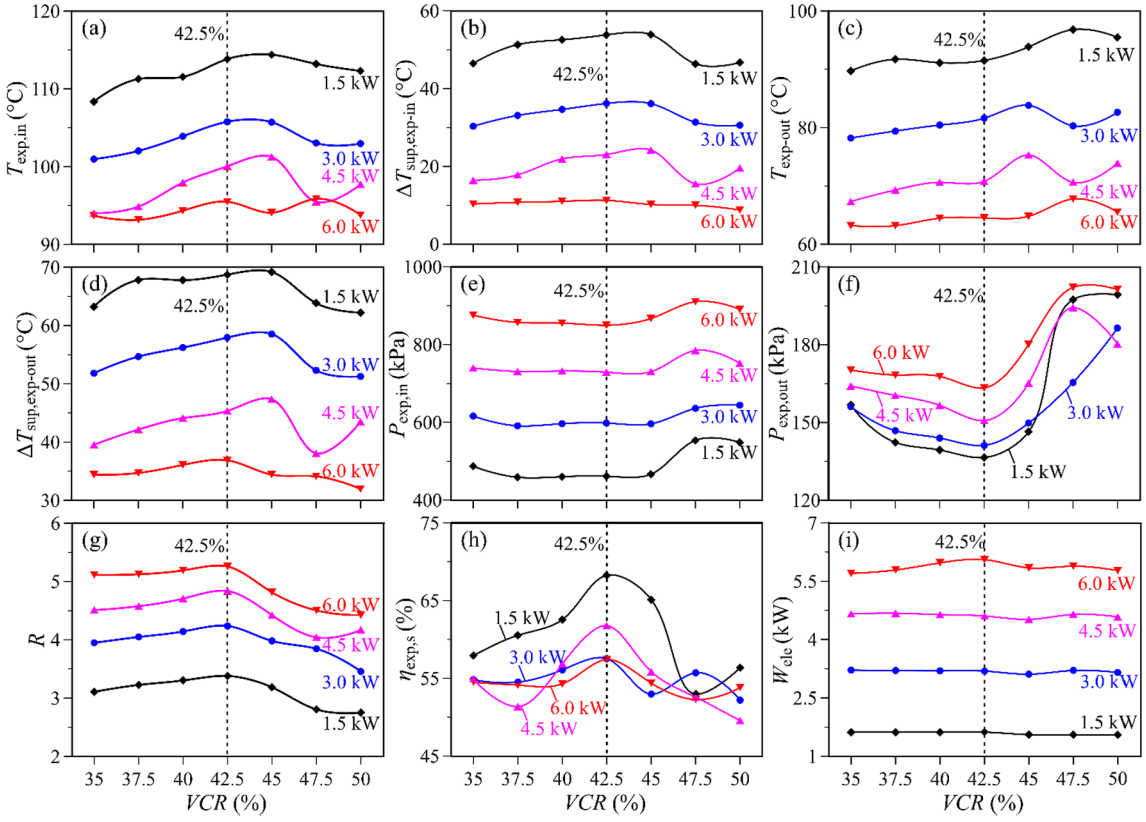


**Fig. 5.** Parameters and performance of expander versus *VCR* at $T_{oil,in}$ = 115.1 °C, $n_{exp}$ = 3000 rpm, $V_{oil}$ = 13.19 $m^3$/h, $V_w$ = 12.44 $m^3$/h.

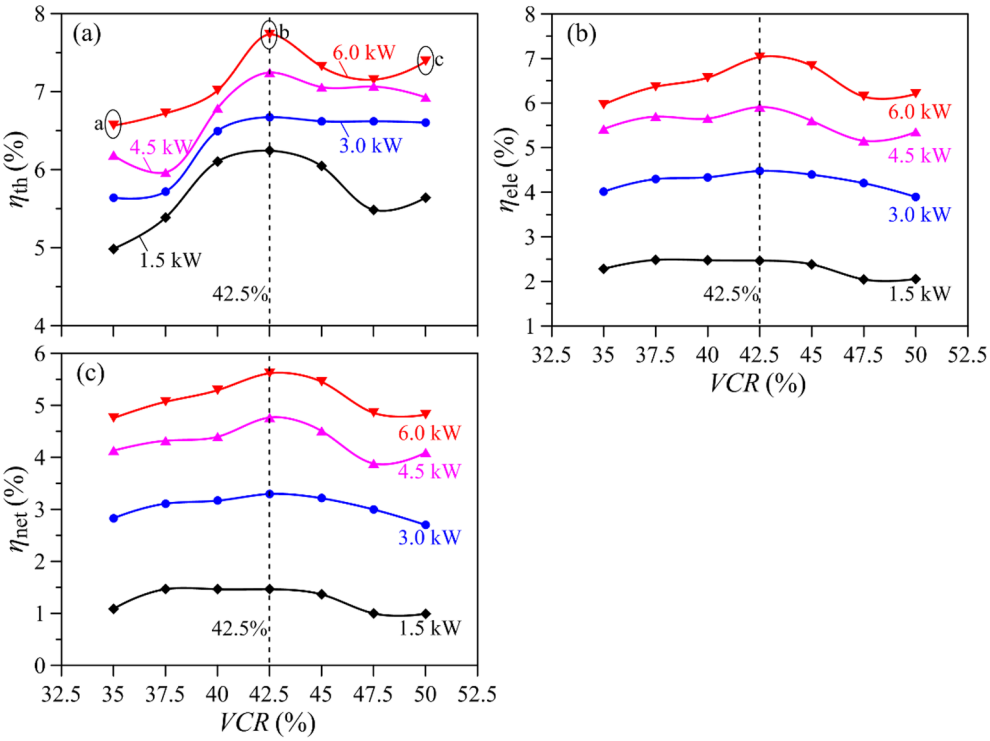


**Fig. 6.** Thermal efficiencies versus *VCR* at $T_{oil,in}$ = 115.1 °C, $n_{exp}$ = 3000 rpm, $V_{oil}$ = 13.19 $m^3$/h, $V_w$ = 12.44 $m^3$/h.

at 3000 rpm and electric loads are in the range of 1.5–6.0 kW. In this study, the internal volume of ORC unit is 113.07 L, measured by weighting method using water as the working fluid. The effects of seven working fluid charge ratios covering the range of 35–50% are examined. It is observed that the ORC system can only successfully operate at working fluid charge ratios from 35% to 50%. For lower charge ratios, the working fluid could not flow back into the liquid tank. For higher charge ratios, the expander back pressure increases significantly. When the charge ratio is 52.5%, the expander back pressure is 890.4 kPa and it could not start to rotate.

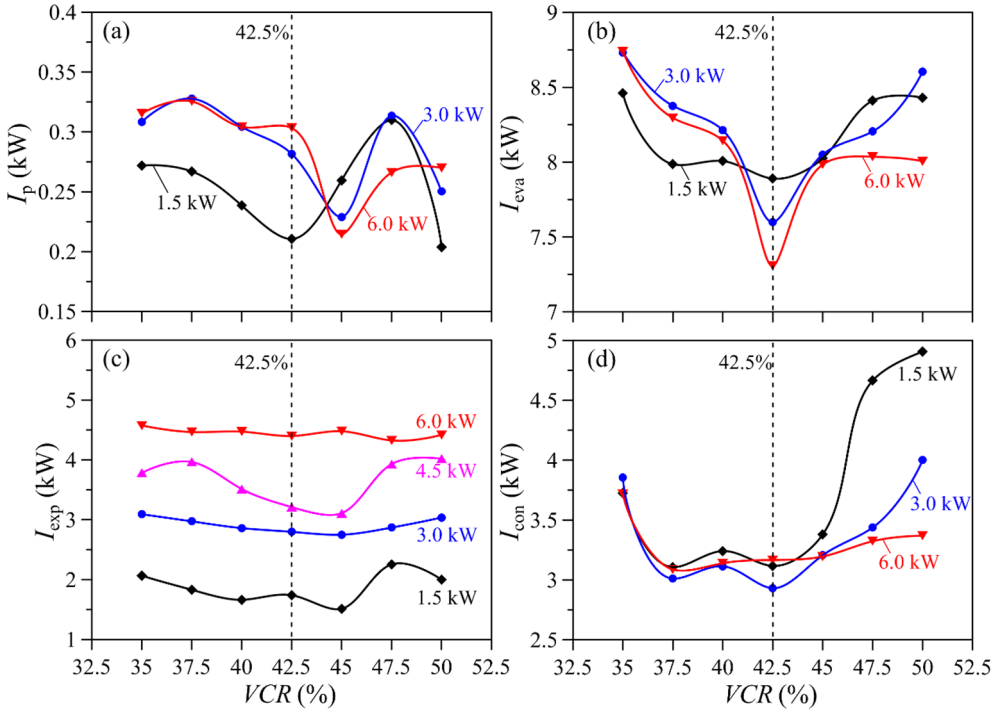


**Fig. 7.** Exergy destruction of the major components versus *VCR* at $T_{oil,in}$ = 115.1 °C, $n_{exp}$ = 3000 rpm, $V_{oil}$ = 13.19 $m^3$/h, $V_w$ = 12.44 $m^3$/h.

At the working fluid charging process before testing, most importantly, the non-condensable gas should be initially removed in the closed ORC unit before R245fa liquid is charged into the system. The liquid tank bottom of the ORC system is connected to a vacuum pump and an organic liquid bottle via a tee valve. Initially, the vacuuming process is performed with the corresponding pipeline open. The vacuuming process lasted 2 h. Then, the vacuuming pipeline is turned off, and the charging pipeline is open by switching the valve. The R245fa liquid is automatically flowing from the high pressure organic liquid bottle to the liquid tank of the ORC system. The weight of bottle is measured before and after the charging process. In such a way, the working fluid charge amount is obtained.

## 3. Results and discussion

### 3.1. Effect of VCR on ORC system performance

#### 3.1.1. Pump performance

Fig. 4 shows the operating parameters and performance of working fluid pump versus *VCR* at various loads. The mass flow rate of R245fa firstly exhibits the slowly decline with *VCR*, reaches the minimum mass flow rate at *VCR* = 42.5%, and then goes up (see Fig. 4a). At the specific *VCR*, more loads can be adapted with the increasing flow rate, which could increase the vapor pressure at expander inlet. The R245fa mass flow rate is mainly affected by the pump inlet pressure as it is directly related to the backpressure of the expander. Thus, the higher pump inlet pressure implies the higher R245fa mass flow rate. In Fig. 4b and c, it can be seen that the pressures at pump inlet and outlet are relatively stable, showing much more slowly decrease with *VCR* firstly, and there also exist minimum values at *VCR* = 42.5%. When the *VCR* is higher than 42.5%, pressures at pump inlet and outlet increase rapidly, indicating the increase in the expander backpressure. As a result, the pumping power also increases (show in Fig. 4d). Fig. 4e identifies the effect of *VCR* on the pump isentropic efficiency at various loads. It is seen that the pump isentropic efficiency generally shows an increasing trend with the increasing *VCR*. In this study, the working pump is a positive displacement diaphragm pump, so that the efficiency is affected by deviation of rated operating.

#### 3.1.2. Expander performance

Fig. 5 shows operating parameters and performance of the expander versus *VCR* at various loads. In Fig. 5a and b, the vapor temperature and superheating at expander inlet firstly gradual increase and then decrease with the *VCR*, existing the maximum values at *VCR* = 42.5%. Besides, the vapor temperature and superheating at expander inlet decreased with the increasing external loads as they are determined by the heat transfer in the evaporator. Based on the heat transfer rules for heat exchanger with fixed area, it can be inferred that, for a given flow rate and inlet temperature of the conductive oil, the lower R245fa mass flow rate lead to the decrease in the heat transfer rate, but the increase in the vapor temperature and superheating at the evaporator outlet.

Fig. 5c and d shows the variations of vapor temperature and superheating at expander outlet versus *VCR*. The vapor temperature gradually increases with the *VCR*, but the vapor superheating first decreases and then increases with the *VCR*. For a specific working fluid charge ratio, it can be observed that the vapor temperature and superheating at expander outlet decrease with the increasing external loads. The vapor temperature and superheating at expander outlet are affected by the combined effects of the inlet temperature, outlet pressure and isentropic efficiency of the expander. The higher inlet temperature and the larger isentropic efficiency of expander resulting in a higher vapor temperature and superheating at expander outlet. However, the outlet pressure behaves a negative effect on the vapor temperature and superheating at expander outlet.

Fig. 5e and f shows the variation of pressures at expander inlet and outlet. Pressures change slowly with *VCR* varying from 35% to 42.5% while rise faster as *VCR* value is higher than 42.5%. The expander outlet pressure is mainly determined by the heat transfer in the condenser. The rapid increase in the expander outlet pressure indicated the heat transfer in the condenser is weakened. The expander inlet pressure is determined by the expander outlet pressure and the load in the present study. Thus, it can be seen that the expander inlet pressure increases with the increase in expander outlet pressure and electric load. Moreover, the comparatively faster change of pressure at expander outlet

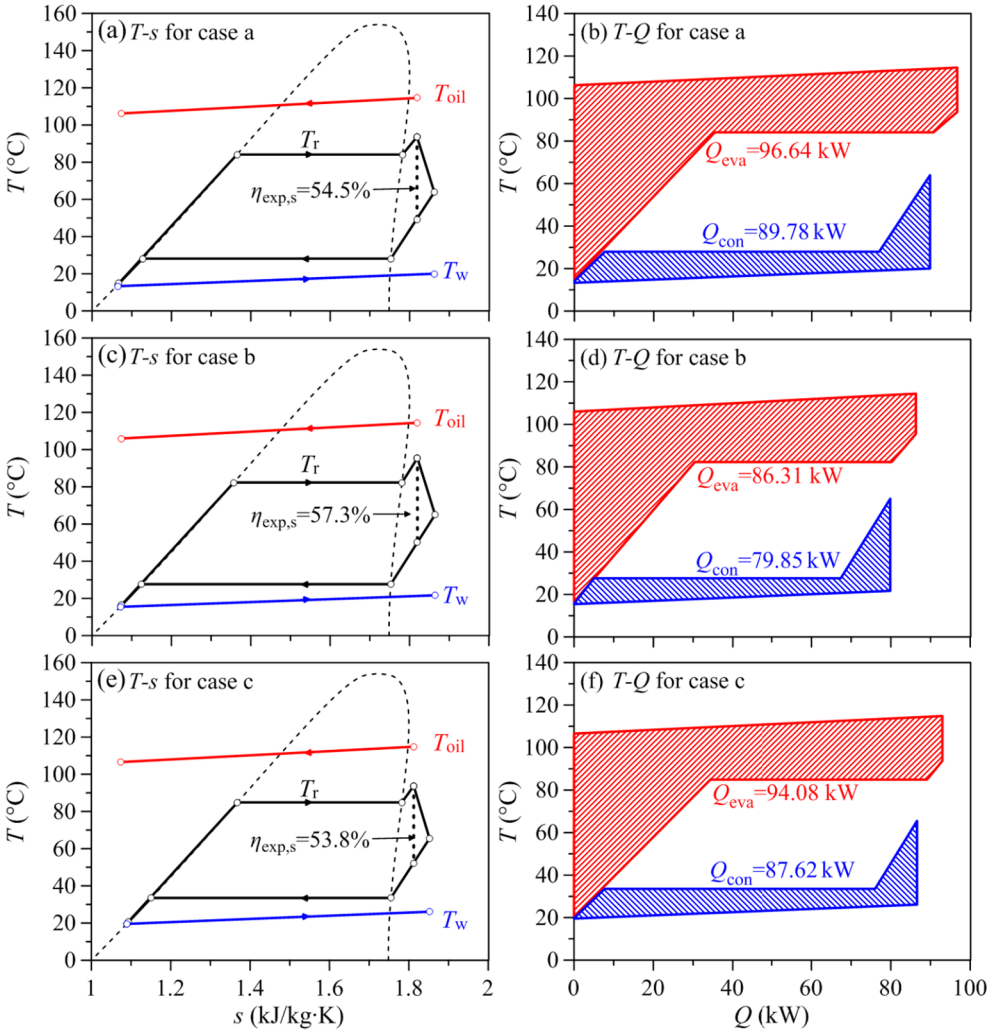


**Fig. 8.** The *T-s* and *T–Q* curves at the three points of a, b and c in Fig. 6a.

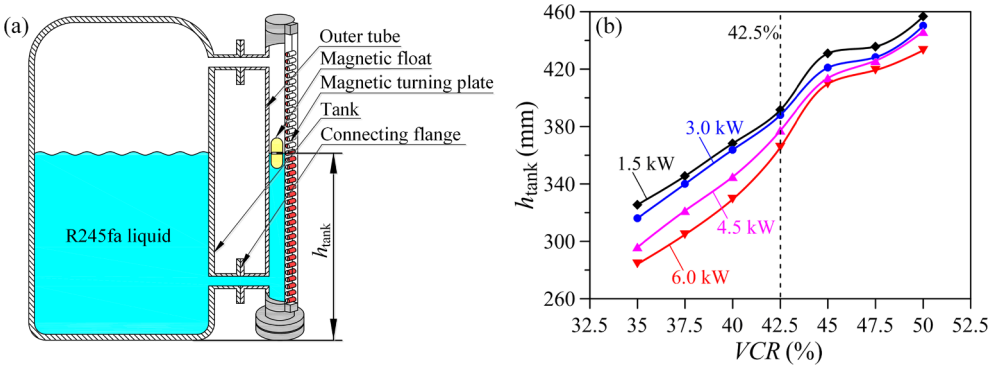


**Fig. 9.** (a) Principle of liquid height $h_{tank}$ measurement and (b) $h_{tank}$ versus *VCR* at $T_{oil,in}$ = 115.1 °C, $n_{exp}$ = 3000 rpm, $V_{oil}$ = 13.19 $m^3$/h, $V_w$ = 12.44 $m^3$/h.

than those at inlet yielding the opposite trend of pressure ratios across the expander (see Fig. 5g). The maximum pressure ratio is 5.26, which occurred at *VCR* = 42.5% and *Load* = 6.0 kW.

Fig. 5h identifies the effect of working fluid charge ratios on the expander isentropic efficiency. The isentropic efficiency of expander exhibits an approximate parabola relationship against the *VCR*. The maximum isentropic efficiency appears at *VCR* = 42.5%, indicating the expander has the best performance. With the increase in vapor temperature and superheating at expander inlet, the vapor density decreased to reduce fluid leakage in expander. It improves the expander isentropic efficiency. Fig. 5i shows the measured electric power. For a given external load, the electric power maintains a steady state under different working fluid charge ratios. At the same time, more electric power is generated with increases of external loads. Our previous finding notes an optimal vapor superheating of about 10 °C to achieve highest electric efficiency [34,35]. A quasi-saturation state vapor may entrain a large number of small droplets, which hit channel walls of expander to worsen expander performance. Therefore, the load is controlled no more than 6.0 kW in this study.

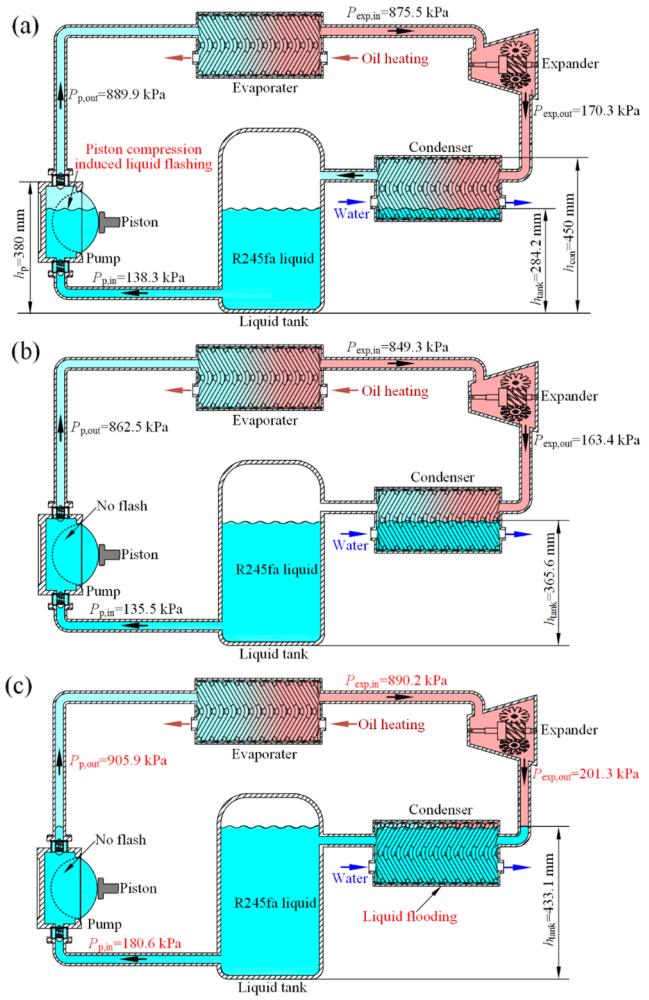


**Fig. 10.** Liquid level height of major components at the three points of a, b and c in Fig. 6a.

### 3.1.3. Efficiencies

Fig. 6 shows the system efficiencies versus *VCR* at various loads. The thermal efficiency ($\eta_{th}$), electric power efficiency ($\eta_{ele}$) and net efficiency ($\eta_{net,ele}$) are defined in Eq. (7)–(9). Because various exergy destructions exist during the thermal to mechanical power conversion and the mechanical power to electricity conversion. Among the three system efficiencies, the thermal efficiency is the largest, and the net efficiency is the lowest but it is more interest to users. All of them are expressed as parabola relationships against the *VCR*. The maximum efficiencies always appear at *VCR* = 42.5% due to the improved expander performance. The maximum thermal efficiency, electric power efficiency and net efficiency are 7.74%, 7.03% and 5.62%, respectively.

It is noted that the off-design operation of the generator and the ORC system has a negative effect on the generator efficiency. The thermal efficiency is 6.24% and the electric power efficiency is only 2.47% at *Load* = 1.5 kW and *VCR* = 42.5%. Therefore, the selection of generator should be match with the ORC system capacity to reduce the irreversible loss in mechanical power to electricity conversion process which could significantly improve the electric power efficiency. In this study, the ORC system has the relatively superior match among the expander performance, the external loads and the system capacity at *Load* = 6.0 kW and *VCR* = 42.5%.

### 3.2. Thermodynamic analysis

Fig. 7 shows the exergy destructions of the four main components versus *VCR* at various loads. It is seen that the pump has the smallest exergy destruction and exhibits quite gentle change with increasing *VCR* (see Fig. 7a). And the expander exhibits the relatively stable profile, indicating the limited variation with the *VCR*. Thus, the exergy destruction of the evaporator and the condenser determines the system performance. The exergy destructions of the heat transfer processes in the evaporator and condenser first decrease and then increase with the *VCR*, and there also exist minimum values at *VCR* = 42.5% (see Fig. 7b and c), indicating the least irreversible losses and highest efficiencies at *VCR* = 42.5%.

Three points in Fig. 6a corresponding to *VCR* = 35.0%, 42.5% and 50% at 6.0 kW external load are picked out to studies how the *VCR* affect the exergy destructions. The corresponding *T-s* and *T-Q* curves are plotted in Fig. 8. Generally, the *VCR* contributes to the higher vapor temperature and superheating degrees at expander inlet as well as the lower pressure at expander outlet in case of *VCR* = 42.5% while the inlet pressure of the expander is relatively stable. Thus, the higher pressure ratio across the expander lead to the higher expander performance. The mass flow rate of R245fa is decreased to adapt the constant external loads. Consequently, the thermal loads of the condenser and evaporator are decreased and it is the principal reason to reduce the dissipation for heat to power conversion in heating and cooling process

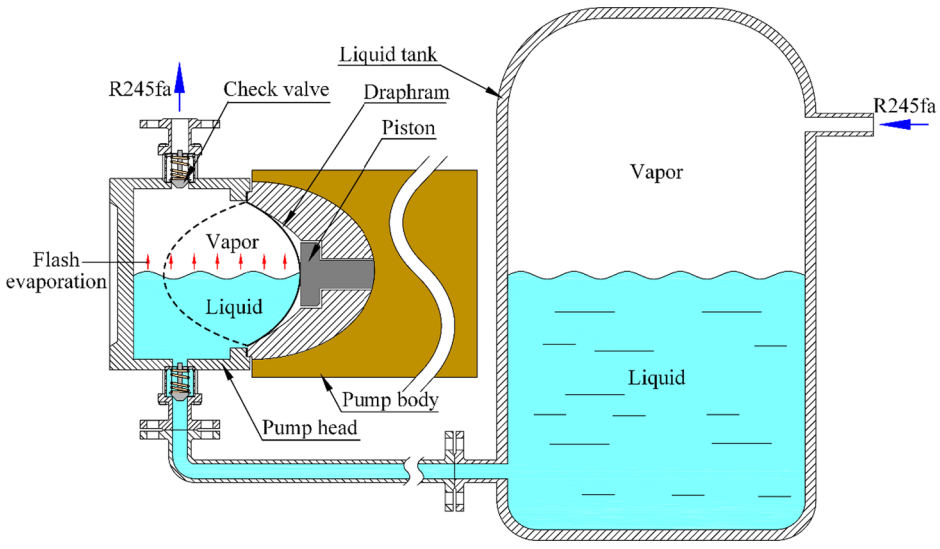


**Fig. 11.** Flash evaporation mechanism in the pump.

to reduce the exergy destructions of evaporator and condenser, while operating parameters are almost constant. The lower outlet pressure of the expander results in the smaller temperature difference of pinch point in the condense, also indicating the smaller dissipation for heat to power conversion in cooling process to reduce the exergy destructions of condenser. Thus, the case of *VCR* = 42.5% has the minimum exergy destruction and the highest efficiency during the thermal to power conversion process.

### 3.3. Pump cavitation and liquid flooding in condenser

Fig. 5e and f shows that the pressure at expander inlet is not sensitive to the variation of the *VCR*. Therefore, the area of preheating section in evaporator, corresponding to the liquid holdup of evaporator, has quite limited change with the *VCR* at a given load. The *VCR* mainly affect liquid holdup of the tank and condenser.

We measured the liquid level in the tank by a magnetic floater liquid level meter to study the effect of *VCR* on liquid holdup of the tank and condense, as shown in Fig. 9. The zero point of the liquid level meter points to the bottom of the tank. Fig. 9b shows the liquid level heights of tank versus the *VCR* at various load capacity. The liquid levels of tank increase with the increased in charge ratios while decrease with the increased in external loads. The measured liquid level of the tank is 365.6–390.4 mm at *VCR* = 42.5%. The diameter of tank is 360 mm. Once the charge ratio is increased by 2.5%, the liquid levels of tank will rise by nearly 20 mm. The volume change of the charging working fluid is equal to that of the R245fa liquid in the tank. Larger external loads lead to the higher pressures at expander inlet and outlet, yielding the larger areas of preheating section in evaporator and subcooling section in condenser. Thus, the liquid holdup of evaporator and condenser increases, and the liquid level of tank is reduced.

Fig. 10 is the schematic diagram of the liquid levels of major components corresponding to the three points shown in Fig. 6a. The height difference between the top of the pump working chamber and the bottom of the tank $h_p$ is 380 mm, and the height difference between the top of the condenser and the bottom of the tank $h_{con}$ is 450 mm. The liquid levels of tank $h_{tank}$ are 284.2 mm, 365.6 mm and 433.1 mm at *VCR* = 35.0%, 42.5% and 50%, respectively (Fig. 10a–c). It is seen that the pump working chamber can not be completely submerged at *VCR* = 35.0%, which causes the pump cavitation and we will discuss this phenomenon in the next section. When the working fluid charge ratio is higher than 42.5%, liquid flooding occurs in the condenser. Consequently, the condenser effective heat transfer area is reduced, yielding the higher pressure at expander outlet. Meanwhile, the gravity pressure drop caused by the actual liquid level height difference between the liquid tank and the condenser also causes the larger pressure drop of the condenser. As a result, the expander performance is weakened. A higher mass flow rate of 245fa is needed to provide enough inlet pressure of the expander to balance the external load. It means the heat transfer loads of the evaporator and the condenser both become larger. However, the increased expander outlet pressure enlarges the subcooling section in the condenser, reduces the effective heat transfer area for the precooling and two-phase section. Thus, the heat transfer capacity of the condenser becomes lower. This contradiction between the increasing heat transfer load and the decreasing heat transfer capacity will reduce the system performance and more severely, will result that the expander cannot be started when the *VCR* is higher than a certain value. The limit value of the *VCR* in the present study is 52.5%, which we have mentioned in Section 2.3. I can be temporarily concluded that the liquid flooding in the condenser should be avoided in the ORC design.

Herein, the schematic diagram of the pump used in the present study is shown in Fig. 11 to analysis the mechanism of pump cavitation at the lower charge ratios. The previous studies [34,46–47] noted that a least liquid subcooling of 4.4 °C is necessary to avoid pump cavitation. However, if the working chamber could not be completely submerged with the organic fluid liquid, the pump cavitation would still happen at a larger subcooling degree. In this study, the liquid subcooling at pump inlet is kept above 12 °C. The pump cavitation can be observed at the lower charge ratios. According to the heights of each component, the pump working chamber could not be completely submerged while *VCR* is less than 42.5%. Because the organic fluids like R245fa has a very low boiling point, the R245fa liquid in the pump was flashing during the pump piston reciprocating motion, which causes pump cavitation. The pump cavitation results in the unstable flow the working fluid, the higher pump consumed power and a short life time of the pump. Thus, it is necessary to avoid pump cavitation during the system design by adjust the heights of the pump and the liquid tank to ensure the pump working chamber to be completely submerged.

It should be pointed out that different ORC systems may have different operating range and optimal *VCR* due to the adopted types of heat exchanger. In this study, the plate heat exchangers were used as the evaporator and condenser. Compare with the fin-tube and shell-tube heat exchangers, the plate heat exchangers have higher heat transfer coefficient and convenient setting. It means the heat transfer areas of the evaporator and the condenser both become smaller for the plate heat exchangers. Thus, the liquid holdup of the heat exchangers reduced which will enlarge the working fluid charge ratio at the same charge amount. However, for a specific ORC system, the operating parameters, such as external load, temperature of working fluid and heat source, have limited effect on the operating range and optimal value of *VCR*. As seen in Fig. 9, once the external load is increased by 1.5 kW, the liquid levels of tank will reduce by 8.86 mm on average and it just about 0.79% of the ORC unit internal volume.

## 4. Conclusions

In this paper, the operation and performance of a 7.5 kW scale ORC system with different working fluid charge ratios are experimentally investigated at heat source temperature of 115 °C. The tank liquid height is measured to explore the liquid holdups of the components. Pump cavitation and condenser flooding mechanisms are analyzed. The major results obtained from this study are summarized as following:

(1) The ORC system can successfully operate at the working fluid charge ratio ranging from 35% to 50%. The optimum working fluid charge ratio is 42.5%. The maximum system thermal, electric power and net efficiencies at this working fluid charge ratio are 7.74%, 7.02% and 5.62%, respectively.
(2) When the working fluid charge ratio is higher than 42.5%, liquid flooding occurs in the condenser. The pressures at expander inlet and outlet increase while the vapor temperature and superheating at expander inlet decrease. As a result, the reduced expander isentropic efficiency and the larger pump consumed power lead to the lower ORC system efficiencies.
(3) Pump cavitation was observed as the pump working chamber could not be completely submerged when the working fluid charge ratio is less than 42.5%. It causes the unstable fluid flow and operation of the system. The life time of the pump is also shortened. To achieve better performance of the ORC system, the working fluid charge ratio should not only ensure the pump to be completely submerged, but also avoid liquid flooding in the condenser.

## Declaration of Competing Interest

The authors declared that there is no conflict of interest

## Acknowledgement

The study was supported by the National Key R&D Program of China (2017YFB0601801), the National Natural Science Foundation of China (51776064), and the Foundation of He'nan Educational Committee (20A470012).

## References


[1] S.P. Guo, et al., A review on the utilization of hybrid renewable energy, Renew. Sustain. Energy Rev. 91 (2018) 1121–1147.
[2] K. Alanne, S.L. Cao, An overview of the concept and technology of ubiquitous energy, Appl. Energy 238 (2019) 284–302.
[3] A. Mahmoudi, M. Fazli, M.R. Morad, A recent review of waste heat recovery by organic Rankine cycle, Appl. Therm. Eng. 143 (2018) 660–675.
[4] A. Behzadi, et al., Multi-objective optimization and exergoeconomic analysis of waste heat recovery from Tehran's waste-to-energy plant integrated with an ORC unit, Energy 160 (2018) 1055–1068.
[5] E. Bellos, C. Tzivanidis, Investigation of a hybrid ORC driven by waste heat and solar energy, Energy Convers. Manage. 156 (2018) 427–439.
[6] V.R. Patil, et al., Techno-economic comparison of solar organic Rankine cycle (ORC) and photovoltaic (PV) systems with energy storage, Renew. Energy 113 (2017) 1250–1260.
[7] A. Ramos, et al., Optimisation of a high-efficiency solar-driven organic Rankine cycle for applications in the built environment, Appl. Energy 228 (2018) 755–765.
[8] D. Vera, et al., Biomass gasification coupled to an EFGT-ORC combined system to maximize the electrical energy generation: A case applied to the olive oil industry, Energy 144 (2018) 41–53.
[9] C.Y. Li, et al., Simulation and evaluation of a biomass gasification-based combined cooling, heating, and power system integrated with an organic Rankine cycle, Energy 158 (2018) 238–255.
[10] J. Kalina, M. Świerzewski, R. Strzałka, Operational experiences of municipal heating plants with biomass-fired ORC cogeneration units, Energy Convers. Manage. 181 (2019) 544–561.
[11] M.C. Bassetti, et al., Design and off-design models of a hybrid geothermal-solar power plant enhanced by a thermal storage, Renew. Energy 128 (2018) 460–472.
[12] A.H. Mosaffa, N.H. Mokarram, L.G. Farshi, Thermo-economic analysis of combined different ORCs geothermal power plants and LNG cold energy, Geothermics 65 (2017) 113–125.
[13] S.M. Bina, S. Jalilinasrabady, H. Fujii, Energy, economic and environmental (3E) aspects of internal heat exchanger for ORC geothermal power plants, Energy 140 (2017) 1096–1106.
[14] A. Uusitalo, et al., Experimental study on charge air heat utilization of large-scale reciprocating engines by means of organic Rankine cycle, Appl. Therm. Eng. 89 (2015) 209–219.
[15] J.L. Xu, et al., An actual thermal efficiency expression for heat engines: effect of heat transfer roadmaps, Int. J. Heat Mass Tran. 113 (2017) 556–568.
[16] M.T. White, et al., Computer-aided working-fluid design, thermodynamic optimisation and thermoeconomic assessment of ORC systems for waste-heat recovery, Energy 161 (2018) 1181–1198.
[17] O.A. Oyewunmi, et al., Performance of working-fluid mixtures in ORC-CHP systems for different heat-demand segments and heat-recovery temperature levels, Energy Convers. Manage. 148 (2017) 1508–1524.
[18] J. Kajurek, et al., Selection of refrigerants for a modified organic Rankine cycle, Energy 168 (2019) 1–8.
[19] X.C. Wang, et al., Working fluid selection for organic Rankine cycle power generation using hot produced supercritical $co_2$ from a geothermal reservoir, Appl. Therm. Eng. 149 (2019) 1287–1304.
[20] J. Xu, C. Yu, Critical temperature criterion for selection of working fluids for subcritical pressure organic Rankine cycles, Energy 74 (2014) 719–733.
[21] X.X. Xia, et al., A novel comprehensive evaluation methodology of organic Rankine cycle for parameters design and working fluid selection, Appl. Therm. Eng. 143 (2018) 283–292.
[22] S.Y. Hou, et al., Performance optimization of combined supercritical $CO_2$ recompression cycle and regenerative organic Rankine cycle using zeotropic mixture fluid, Energy Convers. Manage. 166 (2018) 187–200.
[23] Q. Wu, et al., Design and operation optimization of organic Rankine cycle coupled trigeneration systems, Energy 142 (2018) 666–677.
[24] X. Wu, J. Chen, L. Xie, Integrated operation design and control of organic Rankine cycle systems with disturbances, Energy 163 (2018) 115–129.
[25] G.Q. Shu, et al., Scan of working fluids based on dynamic response characters for organic Rankine cycle using for engine waste heat recovery, Energy 133 (2017) 609–620.
[26] S. Li, H.J. Ma, W.Y. Li, Dynamic performance analysis of solar organic Rankine cycle with thermal energy storage, Appl. Therm. Eng. 129 (2018) 155–164.
[27] S.C. Yang, et al., Experimental investigation on a 3 kW organic Rankine cycle for low-grade waste heat under different operation parameters, Appl. Therm. Eng. 113 (2017) 756–764.
[28] M. Usman, et al., Experimental investigation of off-grid organic Rankine cycle control system adapting sliding pressure strategy under proportional integral with feed-forward and compensator, Appl. Therm. Eng. 110 (2017) 1153–1163.
[29] Y. Jang, J. Lee, Comprehensive assessment of the impact of operating parameters on sub 1-kW compact ORC performance, Energy Convers. Manage. 182 (2019) 369–382.
[30] Y. Feng, et al., Experimental investigation of lubricant oil on a 3 kW organic Rankine cycle (ORC) using R123, Energy Convers. Manage. 182 (2019) 340–350.
[31] M. Bianchi, et al., Experimental analysis of a micro-ORC driven by piston expander for low-grade heat recovery, Appl. Therm. Eng. 148 (2019) 1278–1291.
[32] O. Dumont, et al., Experimental investigation and optimal performance assessment of four volumetric expanders (scroll, screw, piston and roots) tested in a small-scale organic Rankine cycle system, Energy 165 (2018) 1119–1127.
[33] Z. Miao, et al., Operation and performance of a low temperature organic Rankine cycle, Appl. Therm. Eng. 75 (2015) 1065–1075.
[34] X.F. Yang, et al., Operation of an organic Rankine cycle dependent on pumping flow rates and expander torques, Energy 90 (2015) 864–878.
[35] S. Cao, et al., Steady and transient operation of an organic Rankine cycle power system, Renew. Energy 133 (2019) 284–294.
[36] T.L. Li, et al., Experimental comparison of R245fa and R245fa/R601a for organic Rankine cycle using scroll expander, Int. J. Energ. Res. 39 (2) (2014) 202–214.
[37] D.K. Kim, et al., Parametric study and performance evaluation of an organic Rankine cycle (ORC) system using low-grade heat at temperatures below 80°C, Appl. Energy 189 (2017) 55–65.
[38] L. Liu, et al., Experimental investigation on the effect of working fluid charge in a small-scale organic Rankine cycle under off-design conditions, Energy 174 (2019) 664–677.
[39] D. Ziviani, et al., Development and a validation of a charge sensitive organic Rankine cycle (ORC) simulation tool, Energies 9 (6) (2016) 389.
[40] L.C. Liu, T. Zhu, J.C. Ma, Working fluid charge oriented off-design modeling of a small scale organic Rankine cycle system, Energy Convers. Manage. 148 (2017) 944–953.
[41] R. Dickes, et al., Charge-sensitive modelling of organic Rankine cycle power systems for off-design performance simulation, Appl. Energy 212 (2018) 1262–1281.
[42] S. Cao, X.B. Ji, J.L. Xu, R245fa condensation heat transfer in a phase separation condenser, Exp. Therm. Fluid Sci. 98 (2018) 346–361.
[43] D. Ziviani, et al., Optimizing the performance of small-scale organic Rankine cycle that utilizes a single-screw expander, Appl. Energy 189 (2017) 416–432.
[44] O. Nematollahi, et al., Experimental study of the effect of brazed compact metal-foam evaporator in an organic Rankine cycle performance: toward a compact ORC, Energy Convers. Manage. 173 (2018) 37–45.
[45] J.P. Holman, W.J. Gajda, Experimental methods for engineers, fourth ed., McGraw-Hill, Nueva York, 1994.
[46] A. Landelle, et al., Performance investigation of reciprocating pump running with organic fluid for organic Rankine cycle, Appl. Therm. Eng. 113 (2017) 962–969.
[47] F. D'Amico, et al., Semi-empirical model of a multi-diaphragm pump in an organic Rankine cycle (ORC) experimental unit, Energy 143 (2018) 1056–1071.